



Temporal variation in the permeability anisotropy behavior of the Malan loess in northern Shaanxi Province, China: an experimental study

Bo Hong^{1,2} · Xi-an Li¹ · Li Wang^{1,2} · Lin-cui Li¹

Received: 27 June 2018 / Accepted: 8 July 2019 / Published online: 19 July 2019
© Springer-Verlag GmbH Germany, part of Springer Nature 2019

Abstract

By analyzing a fresh soil section and soil samples from Yan'an New Area, northwest China, an engineering shallow loess slope was investigated. Temporal variation in the saturated horizontal hydraulic conductivity (K_h) and saturated vertical hydraulic conductivity (K_v) of loess samples were measured using variable head permeability tests. The K_h and K_v values indicate that the loess exhibited permeability anisotropy in space and time, and K_h and K_v at different depths decreased as seepage time increased. K_h -time showed an exponentially decreasing trend, and K_v -time showed a linearly decreasing trend. Analysis of the initial state and micromorphological features of the loess indicate that the orientation of soil particles in the deposition process may be inherently anisotropic. The K_h and K_v values of the loess tended to decrease with depth, as described by an exponential decay model.

Keywords Anisotropic permeability · Hydraulic conductivity · Temporal variation · Microscopic fabric · Exponential decay model (EDM)

Introduction

Water infiltration (e.g., rainfall, irrigation water, and snow-melt) in most loess areas is a common cause of landslides, in which the hydraulic conductivity (i.e., permeability coefficient) of the loess plays an important role. Chinese loess is a special type of soil formed under arid and semiarid climatic conditions (Pye 1984; Gao 1996; Liu and Ding 1998). Unlike many other soils, loess contains abundant silt grains and carbonate components (Sheeler 1968), endowing it with high strength and structural stability in a dry state. Loess is also porous with vertical development joints (Kie 1988); the soil is slightly coherent, sensitive to high pore-water content, and typically nonstratified (Zhuang et al. 2016). Water can infiltrate the soil easily, making it prone to collapse and

leading to geological disasters in different parts of the world (Kie 1988; Rogers et al. 1994; Assallay et al. 1996); in particular, recently, disasters in the China Loess Plateau region have been more serious (Zhuang et al. 2016, 2017, 2018; Hou et al. 2018).

During water infiltration, soil profile characteristics can heavily affect water content redistribution (Kie 1988). The saturated hydraulic conductivity (K_s) is a key soil hydraulic parameter that controls the water infiltration process and determines water distribution, thus governing slope failure. In general, hydraulic conductivity K_s values are assumed to be the same in engineering practice; however, this assumption does not account for variations in K_s values that result from gradually changing soil texture or inhomogeneities (Wang et al. 2018). Therefore, to better describe the seepage field of the loess landslide, it is necessary to enhance understanding of the spatial variation and temporal variation in K_s (Teufel et al. 1993; Messing and Jarvis 1993; Petersen et al. 2008; Hu et al. 2009; Zeng et al. 2013).

As early as 1883, Darwin indicated that soil was anisotropic (Darwin 1883). Many researchers have put forth notable works on different types of soils in various regions worldwide (Sheeler 1968; Pye 1984; Bai and Elsworth 1994; Gao 1996; Assallay et al. 1996; Liu and Ding 1998). The

✉ Xi-an Li
dclixa@chd.edu.cn

¹ School of Geological Engineering and Geomatics, Chang'an University, Xi'an 710054, Shaanxi, China

² Key Laboratory of Mine Geological Hazards Mechanism and Control, Shaanxi Institute of Geological Survey, Xi'an 710054, Shaanxi, China

permeability anisotropy ratio (r_k) has been widely used to describe the anisotropic penetration of soil (Fig. 1); the ratio constitutes the proportion of the hydraulic conductivity to the seepage in the direction parallel to the soil layer, K_h , to the coefficient of permeability to the seepage in the direction perpendicular to the soil layer, K_v , that is, $r_k = K_h/K_v$ (Kenney and Chan 1973; Chan and Kenney 1973; Witt and Brauns 1983; Dudler et al. 1993). The topic of soil permeability ratio has received extensive attention. Scholars often assume that stratified soils contain large permeability anisotropy ratio engineering values, such as in layered foundations, roadbeds, and dam foundations (Chan and Kenney 1973).

In recent years, the increase in strong rainwater in the Loess Plateau of China (Li et al. 2012) has led to the development of shallow loess landslides, especially in the prevailing rainy season (July–September), such as the Heifangtai Loess landslide group (Hou et al. 2018) and the South Jingyang tableland landslide group (Leng et al. 2018; Zhuang et al. 2018). According to survey statistics from Lei (2001), approximately 15,000 landslides have occurred in the Loess Plateau in Shaanxi Province, with a distribution density exceeding six per square kilometer. Most have been shallow surface slips of < 10 m. The proportion of landslides

accounted for more than half the total number of landslides in the area. An important trigger is the infiltration of rainwater into landslides (Zhuang et al. 2017), which has caused serious natural disasters and major ecological and environmental problems, such as soil erosion in the steep loess-mantled landscape (Zhang et al. 2014). Many studies have shown that anisotropic permeation should be considered and is widely present in geomechanics (e.g., asymmetric consolidation (Ai and Cang 2013; Ai et al. 2014)), hydrogeology (e.g., pollutant migration), geological hazards (e.g., slope stability (Fan et al. 2006; Zhang 2011; Wang et al. 2015; Zhang et al. 2018)), foundation pits (Huang et al. 2014), dam foundations (He and Ding 2006; Shakir 2009; Qi et al. 2012), uneven settlement/subsidence (Bai and Elsworth 1994), and underground engineering (Zhang et al. 2015). Shallow landslides are one of the most dangerous geomorphological processes in the Loess Plateau. The problem of loess anisotropic permeability thus warrants close attention.

Many loess researchers have been concerned with anisotropic permeability. For instance, Hao and Li (1988) used a self-developed osmotic apparatus to measure the permeability rate r_k value of a loess sample with a thickness of 30–66 cm ranging from 0.69 to 1.5; Yu (2016) adopted

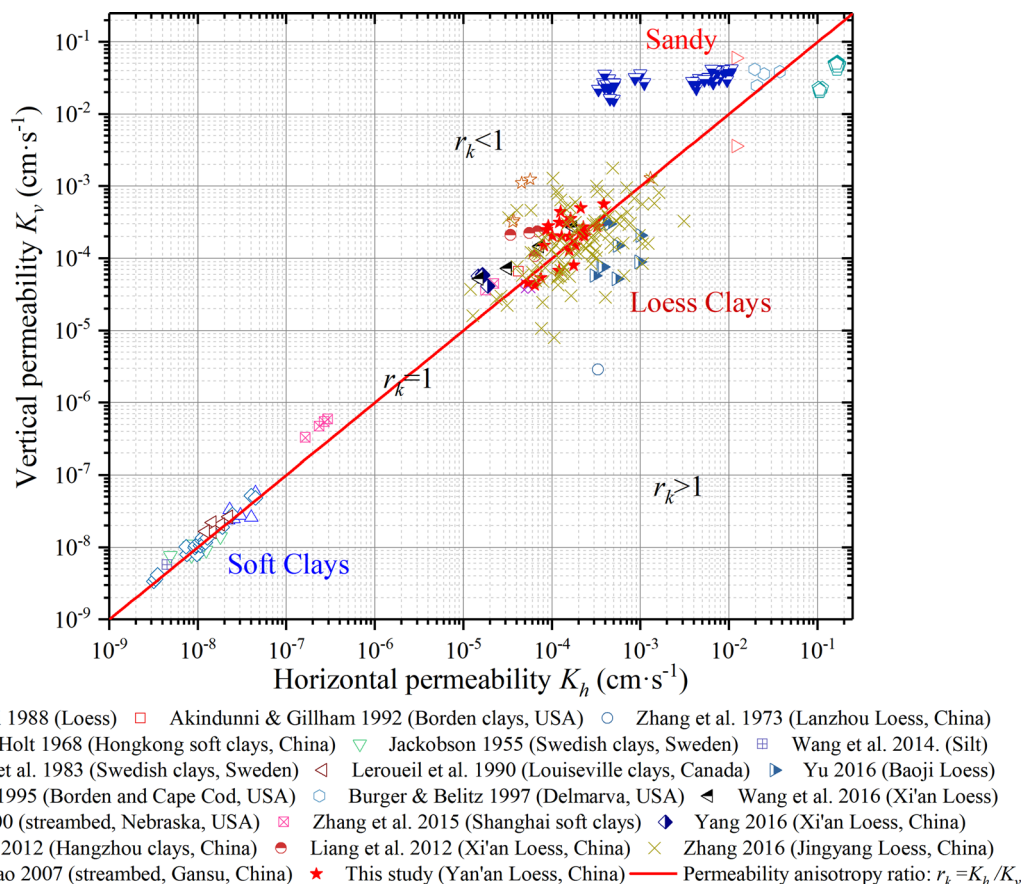


Fig. 1 Permeability anisotropy in soils

the standpipe method, double-ring method, and pumping method. K_h and K_v permeability tests of loess sediments in the loess hilly region in front of the Qinling Mountains in Baoji city, Shaanxi Province, were conducted; the r_k values were all < 1 , and the main seepage direction was vertical. The test results from Liang et al. (2012) showed that the permeability ratio of the undisturbed Malan loess in Xi'an at 10 m was 0.25. Wang et al. (2016) and Yang (2016) used the triaxial permeability apparatus GDS to measure K_h and K_v of the undisturbed loess in Xi'an; the results showed that K_h was higher than K_v , and K_h and K_v decreased with increasing density. Zhang (2016), Lü et al. (2017) and Wang et al. (2018) conducted variable head permeability tests for vertical trench sampling and horizontal adit sampling on the Loess Plateau in South Jingyang tableland, Shaanxi Province. These authors found that the spatial variation in the saturated hydraulic conductivity of the area loess was strong ($r_k < 1$ for the trench and $r_k > 1$ for the adit).

However, the abovementioned studies only investigated spatial variation in permeability anisotropy while ignoring temporal variation. Studies on the spatial and temporal variation in saturated hydraulic conductivity in the loess have not been extensively undertaken. Therefore, the objectives of

the present study are to (1) measure K_h and K_v of the spatial and temporal variation in loess-slope samples; (2) analyze temporal and spatial variation in the vertical and horizontal hydraulic conductivity; and (3) analyze the influence of the initial state of the loess on anisotropic permeability. This investigation will enhance the understanding of the water infiltration process in shallow loess slopes on a local scale, holding great promise for geotechnical design and engineering practice.

Materials and methods

Study site and soil sampling

This study was conducted at the Yan'an New Area I project construction site, located in the middle of the Loess Plateau in China (Fig. 2a, b). The quaternary loess covers the entire area of Late Pleistocene Malan deposits (Zhuang et al. 2018) with a thickness up to 30 m (Li and Li 2017). The loess is now mostly eroded, forming a hilly-gullied geomorphology (Fig. 2b). In recent years, with the advancement of China's urbanization, the population of Yan'an city

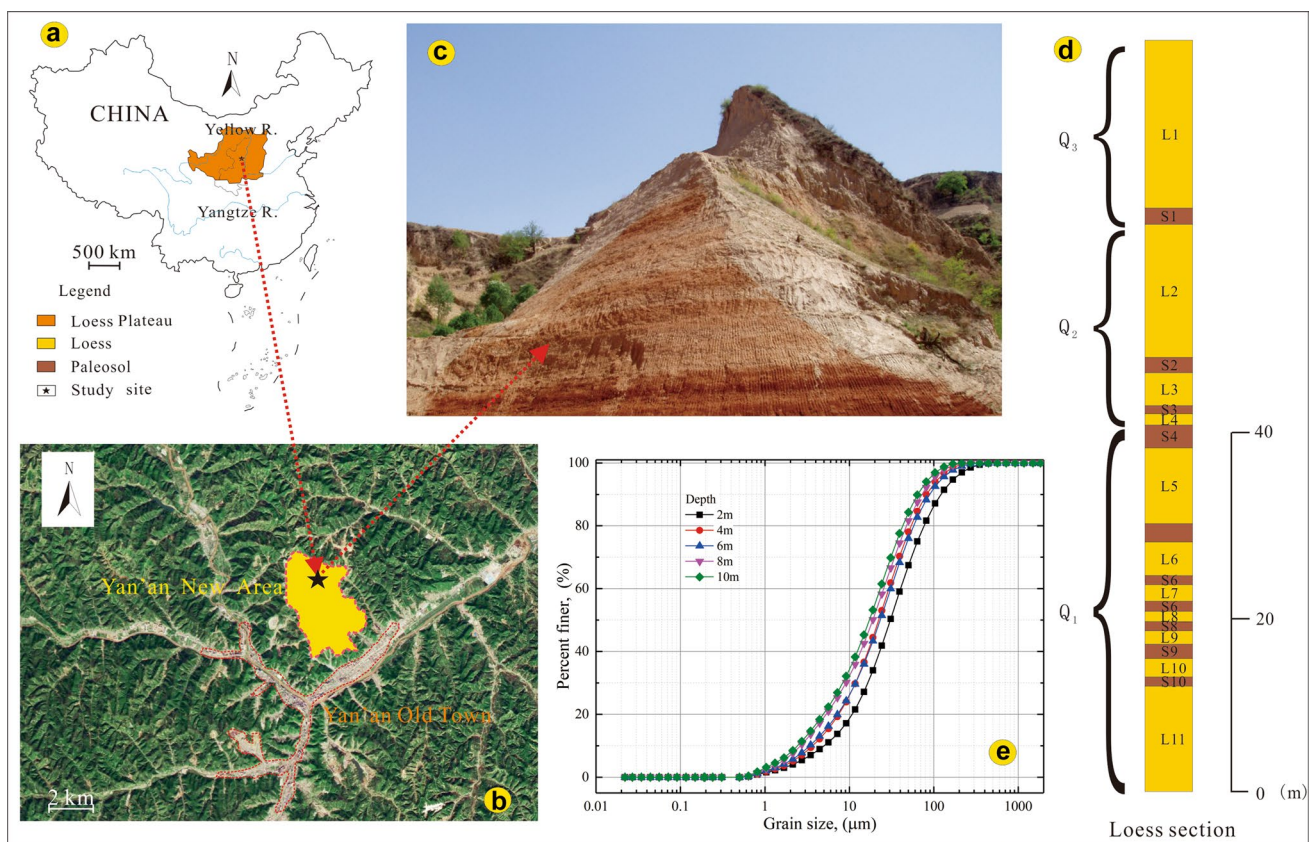


Fig. 2 Overview of the study site: **a** China Loess Plateau map (modified from Liu and Ding (1998)); **b** geomorphology of Yan'an New Area; **c** Engineering Section of Yan'an New Area; **d** Section Column Map of Yan'an New Area; and **e** grain size accumulation curve of the studied soil

has expanded rapidly. It is urgent to expand the framework of large cities and seek new development space (Li et al. 2018), which is beneficial to alleviating the shortage of reserve resources in urban areas and facilitating pulling. The economy continues to grow healthily and improve the living environment. In the first phase of the project, the land use scale is 10.5 km^2 (Fig. 2c), and the total earthwork of the project is $363 \times 10^6 \text{ m}^3$, of which $200 \times 10^6 \text{ m}^3$ is excavated and $163 \times 10^6 \text{ m}^3$ is filled (from the official website of Yan'an Urban and Rural Planning Bureau, China, <http://ghj.yanan.gov.cn>). The Yan'an municipal government adopted the strategy of bulldozing mountains to build a new city to facilitate urban development. Although the urban space has been expanded, it has also produced many hidden geological hazards, namely, shallow loess landslides. Therefore, this study focuses on the anisotropic permeability of shallow Malan loess, which can provide guidance for shallow loess landslide mitigation and project management.

Natural Malan loess samples were collected from the Yan'an New Area, located on the Loess Plateau in China (Fig. 2a). The study site, exposing a maximum vertical section of the stratum layers of 73 m, had a loess-paleosol alternating sequence (Fig. 2d). The sample depths were 2, 4, 6, 8, and 10 m. The authors manually excavated a cylindrical soil sample with a size of $\varphi 135 \times 160 \text{ mm}$ using a shovel in a fresh section of the project and placed it into a sheet iron barrel, marked the buried depth and position, and sealed it with tape (Fig. 3a, b).

Loess properties and mineral components

The basic physical properties of the Malan loess in the five loess samples are tested and are listed in Table 1. Particle size analysis was conducted via a Bettersize2000 laser particle size distribution analyzer (Bettersize Instruments Ltd., Liaoning Province, China, <https://www.bettersize.com.hk/>).

Table 1 Basic physical properties of loess

Property	Value				
Depth (m)	2	4	6	8	10
Water content (%)	12.92	14.83	15.67	16.13	15.87
Nature density (g cm^{-3})	1.67	1.81	1.83	1.87	1.90
Void ratio [dimensionless]	0.84	0.72	0.72	0.68	0.65
Liquid limit (%)	30.6	29.3	30.1	29.9	30.1
Plastic limit (%)	17.5	16.0	16.4	15.9	16.3
Sand ($>0.075 \text{ mm}$, %)	20.49	11.86	13.61	9.34	7.35
Silt ($0.005\text{--}0.075 \text{ mm}$, %)	69.51	74.31	71.72	71.62	72.20
Clay ($<0.005 \text{ mm}$, %)	10.00	13.83	14.67	19.04	20.45

Particle accumulation curves are displayed in Fig. 2e, and the particle composition is shown in Table 1. The shallow loess sediment is a silt-rich clay.

To determine the contents of the mineral composition in the loess, X-ray diffraction was performed with a D/max-2500 X-ray diffractometer manufactured by Japan Rigaku Corporation. According to the quantitative analysis results of Jade 7.0 software, the main minerals in the loess are quartz (Qtz), plagioclase (Pl), potassium feldspar (Or), calcite (Cal), dolomite (Dol), hornblende (Hbl), montmorillonite (Mnt), illite (Ii), and chlorite (Chl) (Table 2). The clay minerals in the loess are mainly illite and chlorite, and the montmorillonite content is low, while kaolinite is almost absent.

Measurement of K_h and K_v

When the cutting ring samples were made in the laboratory, as shown in Fig. 3c, vertical and horizontal specimens were prepared in the same barrel to reliably compare the permeability ratio of the same layer and reduce sample variations. When preparing each sample, a thin layer of Vaseline was smeared onto the inner wall of the cutting ring for



Fig. 3 Soil sampling schematic: **a** manual sampling, marking, and sealing of the samples; **b** sample transportation back to the lab; and **c** preparation of vertical and horizontal cutting ring samples

Table 2 Results of XRD mineral composition (mass percentage, %)

Clay minerals	2 m	4 m	6 m	8 m	10 m
Quartz (Qtz)	53.9	45.3	48.1	45.6	44.6
Plagioclase (Pl)	16.6	18.4	21.8	21.7	19.2
Potassium feldspar (Or)	2.5	3.6	3.8	2.6	6.4
Calcite (Cal)	9.4	12.6	9.6	10.2	10.9
Dolomite (Dol)	1.6	2.1	ND	ND	1.1
Hornblende (Hbl)	ND	2.0	2.2	0.9	0.3
Montmorillonite (Mnt)	2.0	ND	ND	ND	ND
Illite (Ii)	7.0	6.5	7.5	9.5	9.0
Chlorite (Chl)	7.0	9.5	7.0	9.5	8.5

ND, <0.1 or not detected

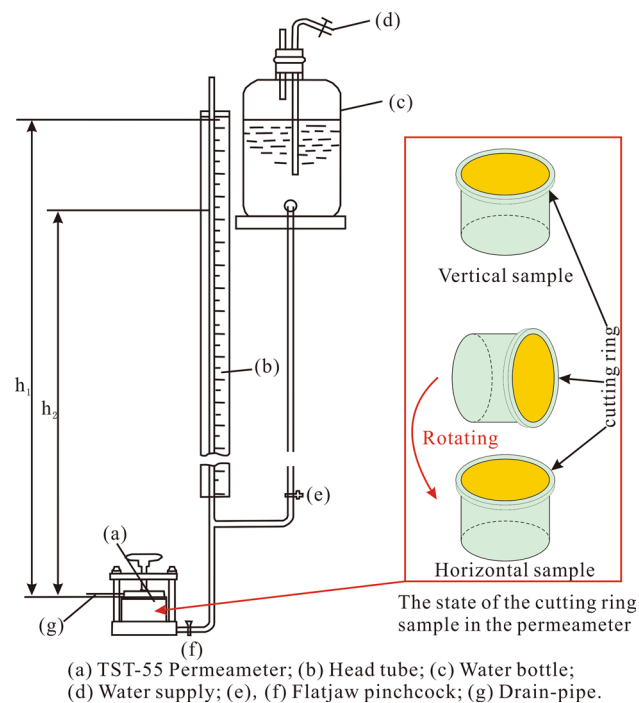


Fig. 4 Variable head test and installation status of the samples

lubrication and to prevent sidewall leakage. Then, a knife was used to level the top surface of the cylindrical soil sample, and the cutting ring was placed on the sample top surface. Next, a cut was made along the outer edge of the cutting ring, and the ring was lightly and evenly pressed until it filled. The sample was then separated along the cutting ring edge and the underlying soil with a knife before leveling the sample at the bottom of the cutting ring to be loaded into the permeameter for testing.

The hydraulic conductivity (K_s) was measured using variable head tests (Fig. 4). Because the samples were prepared horizontally and vertically, the K_s value represented the saturated horizontal hydraulic conductivity (K_h) and the

saturated vertical hydraulic conductivity (K_v). The cutting ring samples that were vacuum-saturated (GB/T 50123-1999) were loaded into the permeameter (Fig. 4a). Flatjaw pinchcocks (Fig. 4d–f) were then opened, and the drain-pipe valve (Fig. 4g) was also opened, so the air in the permeameter could be vented as water passed. When water with no air bubbles overflows evenly through the outlet, the test can begin (GB/T 50123-1999). The start time (t_1) and head (h_1) were recorded along with the end time (t_2) and corresponding head (h_2), and the test was repeated 8–10 times. This data set was saved as T_0 . Then, the flatjaw pinchcocks (Fig. 4d, e) were reopened to let the head rise to a set height again. The experiment was repeated after 1 h, 2 h, 5 h, and 12 h, with the corresponding records marked as $T_1, T_2, T_5,$ and T_{12} . K_h or K_v values were calculated according to Darcy’s law of variable head:

$$K_h \text{ (or } K_v) = \frac{aL}{A(t_2 - t_1)} \ln \frac{h_1}{h_2}, \tag{1}$$

where a is the cross-sectional area (cm^2) of the piezometer tube, L is the height of the loess sample in the cutting ring, and A is the cross-sectional area of the loess sample. For standardization, the permeability coefficient K_T of the experimentally measured water temperature T °C was converted to a permeability coefficient at 20 °C:

$$K_{20} = K_T \frac{\eta_T}{\eta_{20}}, \tag{2}$$

where K_{20} represents the permeability coefficient (cm/s) of the sample at the standard temperature of 20 °C, η_{20} represents the dynamic viscosity coefficient (kPa s) of water at 20 °C, and η_T represents the dynamic viscosity of water at T °C (kPa s).

Scanning electron microscopy (SEM)

The vertical and horizontal small cylinders ($\varphi 10 \times 10$ mm) were prepared, as shown in Fig. 3. The preparation method of the microscopic samples adopted in this work was published by Wang et al. (2010), Li and Li (2017) and Li et al. (2018). SEM photos were carried out with a Quanta FEG450 Environmental scanning electron microscope system manufactured by the American FEI company.

Results and discussion

Basic statistics of K_h and K_v

The variation of loess’s statistical parameters, including the maximum, minimum, mean, standard deviation (SD), and coefficient of variation (CV) of $K_h, K_v,$ and r_k , with

cumulative seepage time along depths, was calculated. The results revealed that during the whole seepage along the soil depth, the mean values, SD, and the CV of K_h and K_v varied from 10^{-5} to 10^{-4} cm s⁻¹, 10^{-7} to 10^{-5} cm s⁻¹, and 0.46 to 2.18, respectively. Moreover, the SD of r_k ranged from 0.01 to 0.12, while the CV of r_k , with a strong variability, were all > 1. Except for the values of T_0 groups and T_{12} groups at 4 m and 8 m depth, the values of r_k of the other groups were all > 1 (Fig. 6d), which means that the saturated hydraulic conductivity of loess in horizontal direction was greater than that in the vertical direction.

Hydraulic conductivity anisotropy can be divided into two types: (1) a vertical hydraulic conductivity that is larger than the horizontal hydraulic conductivity (i.e., $K_h < K_v$) (Zhang et al. 1973; Hao and Li 1988; Liang et al. 2012; Wang et al. 2018) and (2) a horizontal hydraulic conductivity that is greater than the vertical hydraulic conductivity (i.e., $K_h > K_v$) (Al-Tabbaa and Wood 1987; Chapuis and Gill 1989; Widdowson et al. 1990; Leroueil et al. 1990; Akindunni and Gillham 1992; Moench 1995; Burger and Belitz 1997; Chen 2000; Chai et al. 2015).

1. The first case evidence is (a) gravity-driven preferential flow, wherein water flows downward preferentially under gravity and (b) the presence of dominant percolation channels, such as root holes, wormholes, and vertical joints in the loess. Therefore, in the presence of pores and fissures, K_v will be larger than K_h (Chapuis and Gill 1989; Wang et al. 2018).
2. The evidence for the second case can be mainly ascribed to the orientation of soil particles. During the deposition process, layered and flake particles form a layered structure, resulting in K_h higher than K_v (Mast and Potter 1963; Chapuis and Gill 1989; Wang et al. 2016).

Spatial variability in permeability anisotropy varies, as soil properties change. Soils in different regions exhibit large variations in performance due to differences in the soil-forming environment (Hu et al. 2009). The penetration direction is also determined by a certain dominant factor in the soil. For the study area, the direction dependence of soil particles was the dominant factor of permeability anisotropy in the Malan loess-forming process, similar to the results by Wang et al. (2016) regarding the permeability of the Xi'an loess (at 10 m).

Micromorphological features of loess

Figure 5 shows SEM photographs of horizontal and vertical slices of samples with depths of 4 m and 10 m, respectively. It can be seen from Fig. 5 that the granular composition of loess is mainly composed of flat particles, which are mixed with fine particles and clay to form a fabric (or aggregate)

between the soil particles as a whole and the mutual arrangement and relationship between various features. One of the microscopic mechanisms of anisotropy is microscopic fabric anisotropy, and other anisotropy features are the macroscopic manifestations of the microfabric anisotropy (Qian and Huang 2011), which is essentially caused by the directional arrangement of clay mineral particles (Brewer 1972). Burnham in 1970 proposed seven permutations of the microfabrics of different clay particles (see in Fitzpatrick 1993). Although it is difficult to use soil micromorphology to quantitatively describe the overall structure of soil, it is particularly useful in studying the history and development of soil profiles (Brewer 1972).

Figure 5 shows that there are few sharp grains in the Yan'an loess, which may be closely related to the aeolian genesis of the loess (Liu and Ding 1998). The particles are relatively rounded due to the external force in the process of wind transport. There are many microfabrics in the form of A, B, E, F, and G in Fig. 5, which may be related to the deposition–consolidation process of loess. Although particles can be carried by the winter monsoon, the true consolidation process relies on annual summer monsoon rain (Zhang et al. 2012). At the same time, due to the complex electrochemical action of clay minerals, the spatial arrangement of sedimentary particles (i.e., fabrics) is also greatly affected by the chemical composition of sedimentary solution (Moon 1972). The electrolyte concentration of the deposition solution also controls which of the three contact modes is between particles: face-to-face, edge-to-face, and edge-to-edge (Van Olphen 1963). The combination of different particle–particle contact modes necessarily forms different microscopic structures, such as FF associations, which are more likely to form plate-like and sheet-like fabrics (e.g., Fig. 5b–d), while EF and EE association is more inclined to form a messy fabric (e.g., Fig. 5a, e–g). However, in the plastic (wet) state, even a small stress will have a greater impact on the orientation of particles, which tends to move perpendicular to the stress direction in the large plane (Greene-Kelly and Mackney 1970; Brewer 1972; Moon 1972). However, in this wet state, the preferential orientation of the spatial arrangement of sedimentary particles (or fabrics) may only be formed a few meters below the surface soil at the initial stage of consolidation (Meade 1966). Of course, the composition of the deposition solution is also affected by environmental factors such as acid rain and alkali rain.

Therefore, the process of deposition and consolidation of the natural loess layers, the resultant soil particles and structural units often exhibit an orientation in space, particularly flat particles (e.g., platy, sheet, fibrous, and layered), especially for particles with a long axis direction parallel to the ground surface. Over the years, this deposition–consolidation cycle has formed anisotropy in loess structures (Wang et al. 2016).

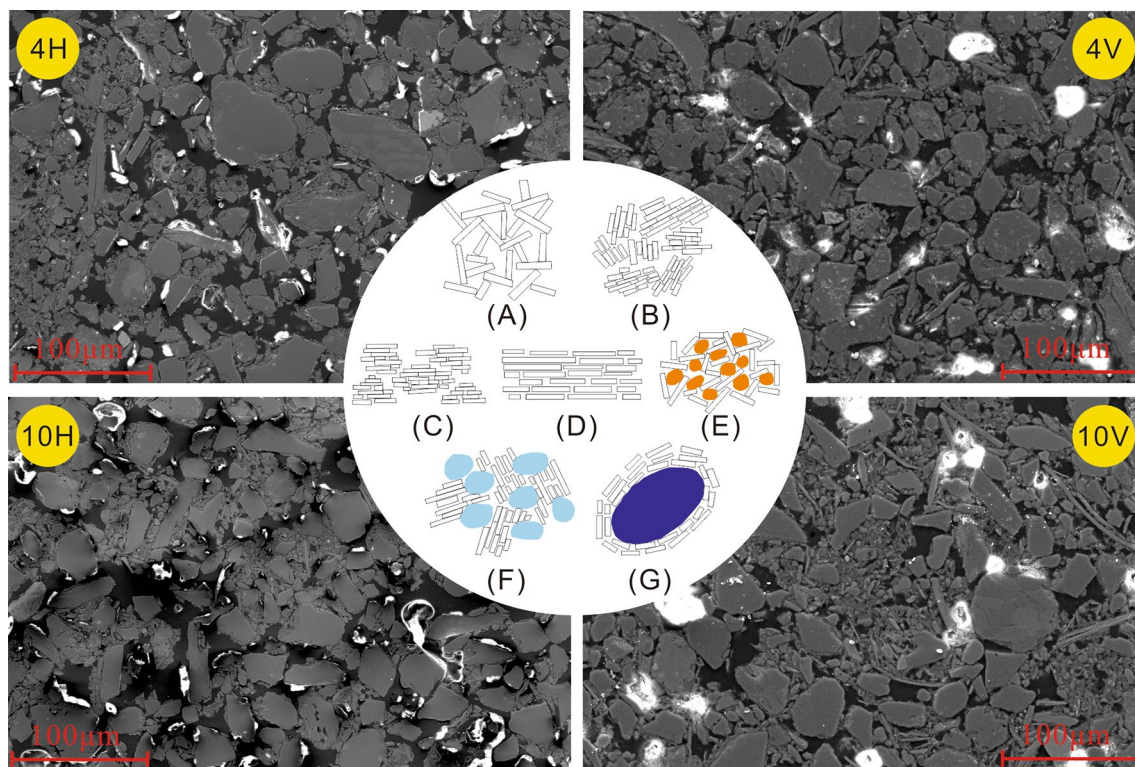


Fig. 5 Arrangement of loess particles: (A) fabric composed of randomly orientated clay particles; (B) fabric composed of randomly orientated domains; (C) fabric of domains in parallel alignment; (D) fabric of parallel orientated clay particles with little differentiation of domains; (E) granular particles of fine silt interfere with the parallel

orientation of the clay particles; (F) randomly orientated domains may occur between grains of coarse silt; and (G) large sand particles with clay particles aligned tangential to their surfaces. (see in Fitzpatrick 1993)

Temporal variation in K_h and K_v

Figure 6a shows that in this study, K_h and K_v at different depths declined as the seepage time increased. K_v decreased rapidly in the T_0 – T_2 stage and then tended to become stable over increasing time, with a decreasing trend in the exponential function ($y = ax^b$) (Fig. 6b). K_h demonstrated a linear decrease ($y = a + bx$) over time (Fig. 6c).

Although substantial time variations in hydraulic conductivity have been found in many places, the vast majority of studies have focused on cultivated soil (approximately 1 m) (Teufel et al. 1993; Petersen et al. 2008; Hu et al. 2009; Zeng et al. 2013). Few studies have been carried out on the regularity of the infiltration time of soil layers below cultivated soil. Leroueil et al. (1990) measured the horizontal hydraulic conductivity of Louisville soft clay at a depth of 9.2 m under cumulative time, showing that the horizontal hydraulic conductivity did not change substantially over time (Fig. 6e).

In vertically saturated seepage, the cement material around the skeleton particles was dissolved, and the fine clay particles migrated as time went on, causing the soil to collapse on a microscale and to clog the seepage channel, so the hydraulic conductivity declined rapidly (Fig. 6b). When

horizontally saturated seepage occurred, the soil also collapsed on the microscale. However, due to the directional arrangement of soil particles, even if a certain point collapsed, it only caused translation due to the limitations of surrounding particles. Therefore, a reduction in the horizontal hydraulic conductivity was not as intense as that in the vertical direction (Fig. 6c).

Figure 6d shows that the permeability ratio r_k increased first and then declined with the seepage time. At a depth of 2 m, the permeability anisotropy ratio reached a maximum of $r_k = 3.52$ after 2 h of percolation; the other depth was essentially a peak r_k when the percolation was close to 5 h. This phenomenon was likely related to soil variation. Higher sand content and fewer clay particles appeared at 2 m (Table 1), and the cementation was poor; therefore, the collapsing deformation in the saturated seepage was relatively short. With an increase in depth, the soil sand content decreased, the clay particle content increased (Table 1), and the cementation effect was good. Therefore, the collapsing deformation in saturated seepage took longer, and the corresponding peak permeability ratio appeared later.

Therefore, why is the vertical and horizontal water conductivity of the Malan loess so varied over time? The answer

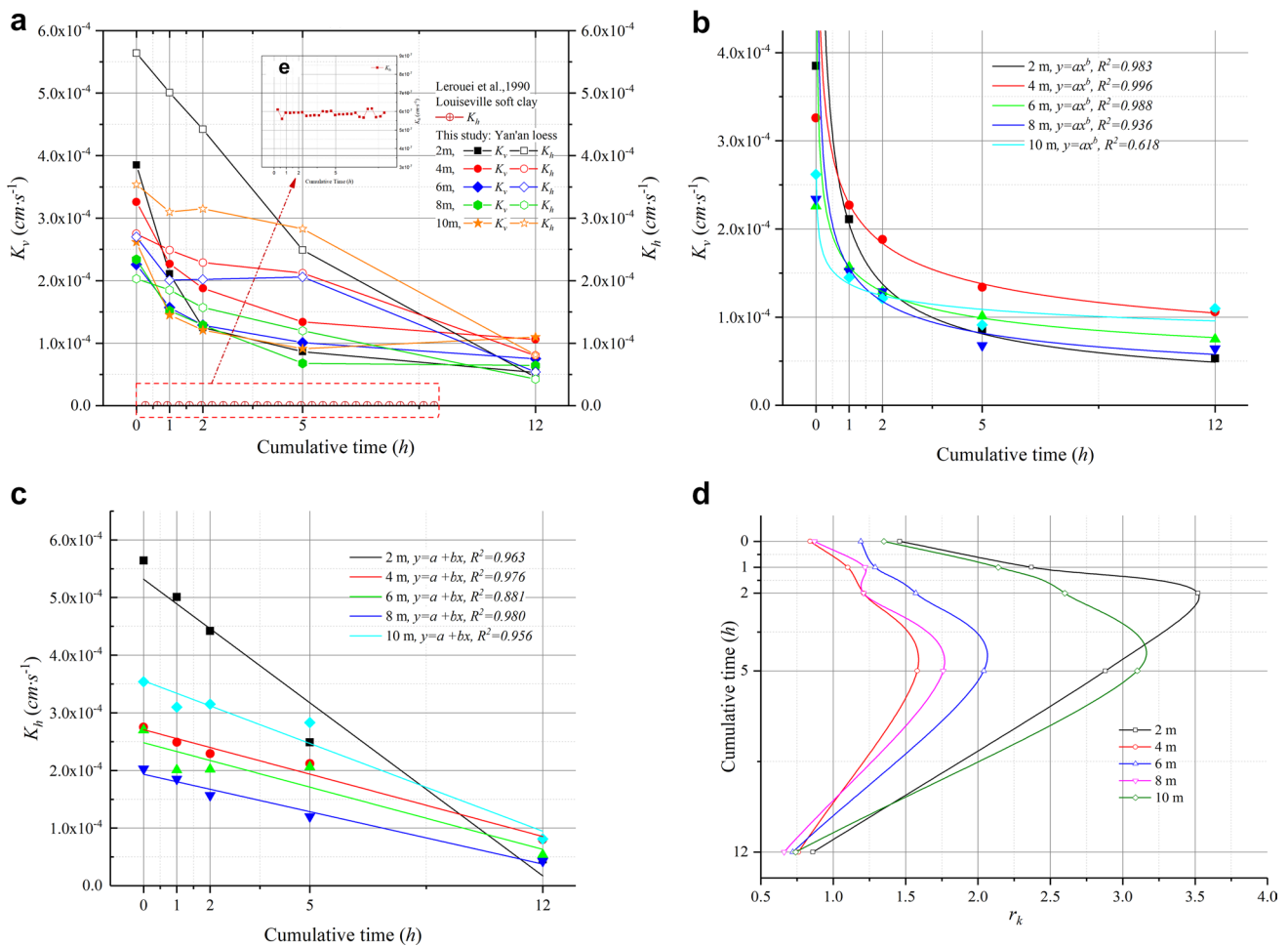


Fig. 6 Temporal variation in K_h and K_v . **a–c** K_h -time and K_v -time relationship; **d** permeability anisotropy ratio r_k -time relationship; and **e** K_h -time relationship. (Leroueil et al. 1990)

may be closely related to the deposition and consolidation of the Malan loess.

Influence of the initial state

The initial state of soil directly affects many physical properties (e.g., initial dry density, initial moisture content, and initial void ratio).

Initial dry density

Figure 7 demonstrates that the vertical and horizontal permeabilities of undisturbed loess decreased with an increase in the initial dry density, and the horizontal hydraulic conductivity was substantially greater than the vertical hydraulic conductivity at the same initial dry density. This result is largely consistent with that by Hao and Li (1988), Liang et al. (2012), Yang (2016), and Wang et al. (2016). Wang et al. (2016) considered that at the same initial dry

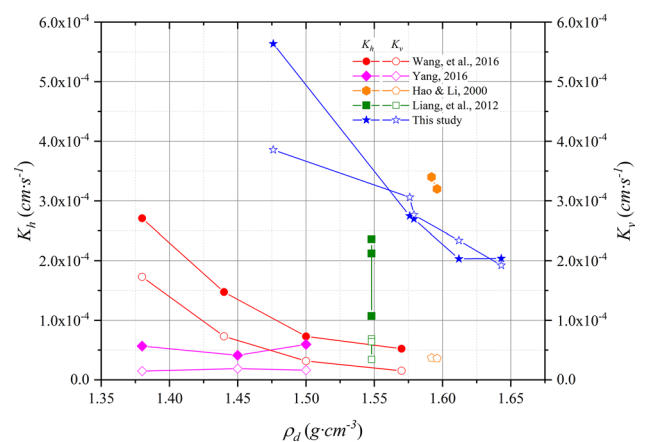


Fig. 7 Relationship between dry density (ρ_d) and K_h , K_v

density, the vertical direction loess grains were more densely arranged than the horizontal grains. Cement material in the horizontal direction mainly filled in intergranular pores, whereas the vertical direction occurred due to many cementitious materials; the skeleton particles were embedded and interconnected in blocks, endowing the intact loess structure with clear anisotropy.

Initial water content

Figure 8 illustrates that as the initial moisture content increased, the vertical and horizontal saturated hydraulic conductivity each tended to decline. The influence of the initial moisture content on the hydraulic conductivity was mainly affected by the location and occurrence state of cementation material along with the effect of cement on the distribution of loess pores and the ratio of effective pore connectivity (Hong et al. 2016; Li et al. 2017).

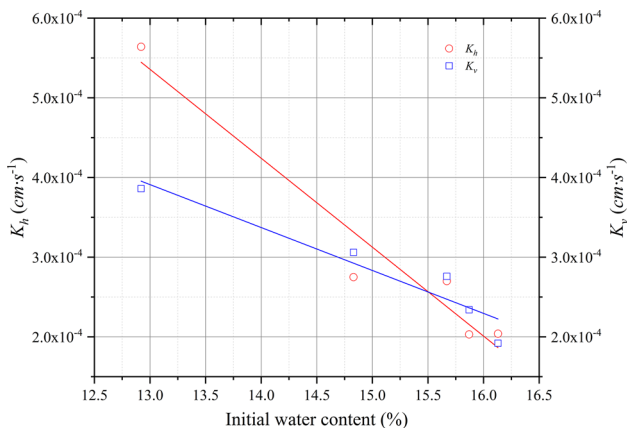


Fig. 8 Respective relations between initial water content and K_h , K_v

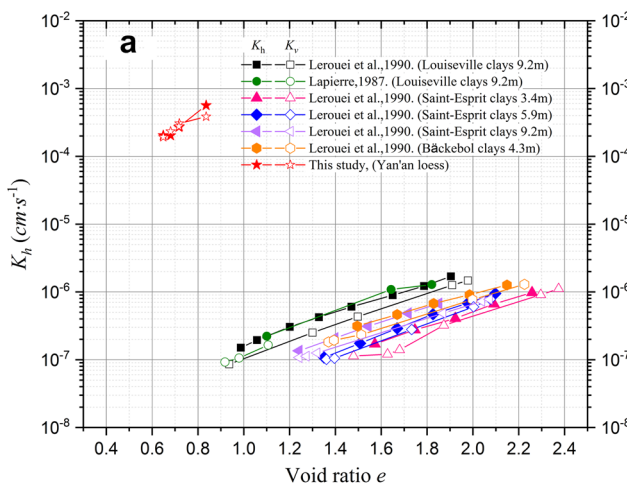


Fig. 9 Relation between saturated hydraulic conductivity (K_h , K_v) and void ratio e

Initial void ratio

In essence, the soil initial dry density directly determined the initial porosity ratio. The greater the dry density was, the smaller the void ratio. Therefore, the effect of the initial void ratio on the hydraulic conductivity was opposite to that of the initial dry density; that is, with an increase in the initial void ratio, the vertical and horizontal saturated hydraulic conductivity each increased (Fig. 9a). As shown in Fig. 9b, the e - $\log K_h$ and e - $\log K_v$ relationships were linear. As in Leroueil’s penetration anisotropy for marine clays, the e - $\log K_h$ and e - $\log K_v$ relationships were essentially parallel (Leroueil et al. 1990). In this study, the e - $\log K_v$ slope of loess was larger than e - $\log K_h$.

K_h and K_v variation with depth

The previous studies have reported that hydraulic conductivity (or permeability coefficient) in aquifers decays with depth (e.g., Jiang et al. 2010; Wang et al. 2018). Many equations describing this phenomenon have been proposed, including theoretical and empirical models. Under special circumstances in either a porous medium or fractured medium, variations in hydraulic conductivity with depth can be simplified to an exponential decay model (EDM) (Jiang et al. 2010; Wang et al. 2018), written as

$$K(z) \approx K_0 \exp(-Az), \tag{3}$$

where $K(z)$ is the hydraulic conductivity at depth z in the aquifer, K_0 is the hydraulic conductivity at the ground surface, and A is the decay exponent indicating the rate of decline. The larger the A value is, the larger the rate of decline. Because hydraulic conductivity K_s decay trends in loess have rarely been investigated (Wang et al. 2018), this theoretical model was used to fit K_h and K_v measurements

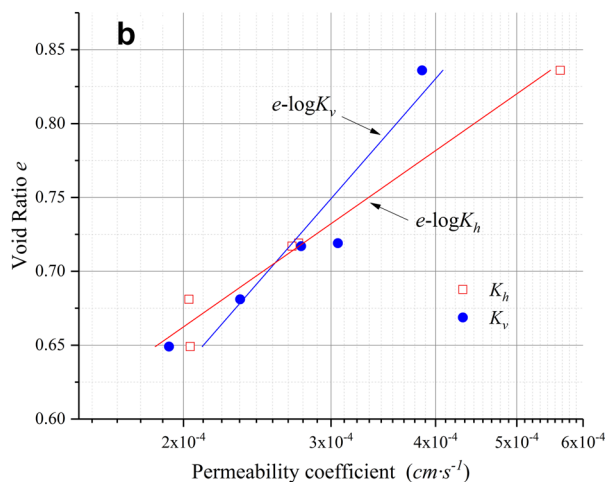
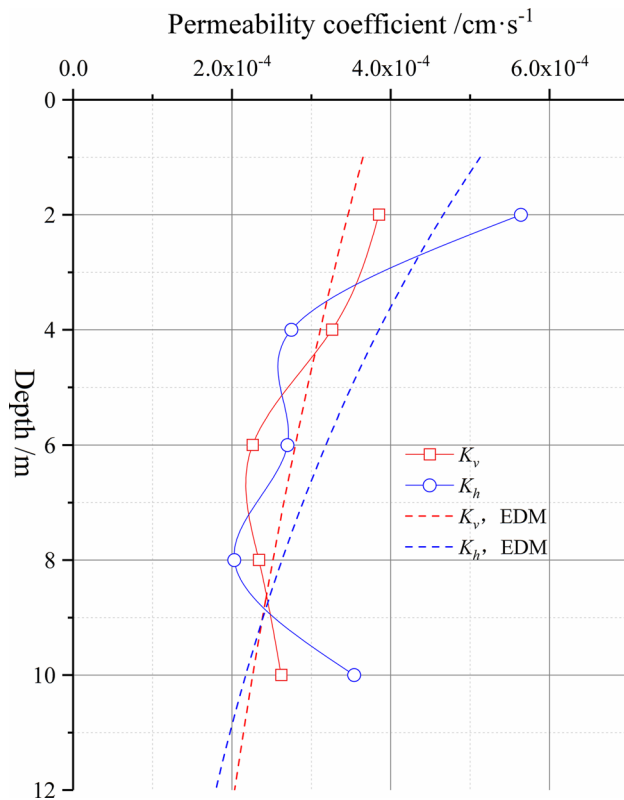


Table 3 K_h and K_v variation with depth in the loess. A is the decay exponent of the EDM

Depth (m)	0–10	
Variable	K_v	K_h
A	0.0532	0.0954
R^2	0.66	0.41

**Fig. 10** Variation in hydraulic conductivity (K_h and K_v) with depth

along the depths in this study. The decay model of the Malan loess was identified. The decay exponent A in each case was determined by the minimum residual sum of squares (Table 3). The fitting plots are shown in Fig. 10.

As shown in Fig. 10, both K_h and K_v decrease with increasing loess depth (Wang et al. 2018), and the correlation coefficient R^2 is 0.41 and 0.66, respectively. This result shows that the exponential decay model for aquifer hydraulic conductivity change analysis can be applied to describe loess, especially the vertical direction. Since the gravity of the overlying soil layer has a compaction effect on the lower layer, the vertical hydraulic conductivity of the loess is attenuated with depth. This process can be considered the result of consolidation of the formation. However, the attenuation of K_h is weak with depth, because the loess pores are a complex system composed of interconnected pores, pores, and fractures, and the preferential orientation of the fabric in the sedimentation–consolidation process also makes that the

pores show significant spatial differences. Macroscopically, at different depths, the hydraulic conductivity demonstrated wide variability (Fig. 10).

Conclusions

Yan'an New Area, in the middle of the Chinese Loess Plateau, contains loess as the most continuous soil in the vertical and horizontal space. By excavating a fresh section and taking loess samples, this study analyzed the K_h and K_v of the loess. Permeability anisotropy of the Yan'an loess demonstrated substantial anisotropy, as evidenced by the K_h and K_v values in space and time. K_h and K_v measurements of the loess samples revealed a decreasing trend over time and an increase in depth; K_h -time showed an exponentially decreasing trend, and K_v -time showed a linearly decreasing trend. The permeability anisotropy ratio r_k values indicated that r_k reached a peak after 2 h of percolation at a depth of 2 m. At other depths, a 5-h r_k was essentially required to reach the peak. This phenomenon may be related to soil variation with depth. The influence of the initial state of the loess (including initial dry density, initial moisture content, and initial void ratio) was analyzed. The loess microfabric was not random but was rather affected by the directional arrangement of the particles during loess deposition, thus leading to the spatiality and temporal variation in the K_h and K_v measurements. The exponential decay model used to analyze the attenuation of the aquifer hydraulic conductivity could be used to describe the variation in K_h and K_v with loess depth. Although the research results are only experimental results for the section of Yan'an New Area, this study serves as a working method for understanding the geotechnical design and engineering practice of shallow loess-slope landslides.

Acknowledgements This study was financially supported by the Natural Science Foundation of China (Nos. 41572264 and 41877225), the Fundamental Research Funds for the Central Universities, CHD (No. 300102268717), and the Key Laboratory of Mine Geological Hazards Mechanism and Control (Nos. KF2017-16 and KF2017-17). The authors would like to sincerely thank the editors, as well as the reviewers of this paper, who provided constructive comments that substantially improved the manuscript.

References

- Ai ZY, Cang NR (2013) Non-axisymmetric Biot consolidation analysis of multi-layered saturated poroelastic materials with anisotropic permeability. *Soils Found* 53:408–416. <https://doi.org/10.1016/j.sandf.2013.04.003>
- Ai ZY, Hu YD, Cheng YC (2014) Non-axisymmetric consolidation of poroelastic multilayered materials with anisotropic permeability and compressible constituents. *Appl Math Model* 38:576–587. <https://doi.org/10.1016/j.apm.2013.06.014>

- Akindunni FF, Gillham RW (1992) Unsaturated and saturated flow in response to pumping of an unconfined aquifer: numerical investigation of delayed drainage. *Groundwater* 30:873–884. <https://doi.org/10.1111/j.1745-6584.1992.tb01570.x>
- Al-Tabbaa A, Wood DM (1987) Some measurements of the permeability of kaolin. *Géotechnique* 37:499–514. <https://doi.org/10.1680/geot.1987.37.4.499>
- Assallay AM, Rogers CDF, Smalley IJ (1996) Engineering properties of loess in Libya. *J Arid Environ* 32:373–386. <https://doi.org/10.1006/jare.1996.0031>
- Bai M, Elsworth D (1994) Modeling of subsidence and stress-dependent hydraulic conductivity for intact and fractured porous media. *Rock Mech Rock Eng* 27:209–234. <https://doi.org/10.1007/BF01020200>
- Brewer R (1972) The basis of interpretation of soil micromorphological data. *Geoderma* 8:81–94. [https://doi.org/10.1016/0016-7061\(72\)90037-7](https://doi.org/10.1016/0016-7061(72)90037-7)
- Burger RL, Belitz K (1997) Measurement of anisotropic hydraulic conductivity in unconsolidated sands: a case study from a shoreface deposit, Oyster, Virginia. *Water Resour Res* 33:1515–1522. <https://doi.org/10.1029/97WR00570>
- Chai J, Jia R, Nie J, Aiga K, Negami T, Hino T (2015) 1D deformation induced permeability and microstructural anisotropy of Ariake clays. *Geomech Eng* 8:81–95. <https://doi.org/10.12989/gae.2015.8.1.081>
- Chan HT, Kenney TC (1973) Laboratory investigation of permeability ratio of New Liskeard varved soil. *Can Geotech J* 10:453–472. <https://doi.org/10.1139/t73-038>
- Chapuis RP, Gill DE (1989) Hydraulic anisotropy of homogeneous soils and rocks: influence of the densification process. *Bull Eng Geol Environ* 39:75–86. <https://doi.org/10.1007/BF02592538>
- Chen X (2000) Measurement of streambed hydraulic conductivity and its anisotropy. *Environ Geol* 39:1317–1324. <https://doi.org/10.1007/s002540000172>
- Darwin GH (1883) On the horizontal thrust of a mass of sand. *Minutes Proc Inst Civ Eng* 71:350–378. <https://doi.org/10.1680/imotp.1883.21802>
- Dudler IV, Golovishnikov VI, Shchetinina AP (1993) Temporal variation of seepage anisotropy of hydraulic-fill soils of hydraulic structures. *Hydrotech Constr* 27:31–37. <https://doi.org/10.1007/BF01545555>
- Fan Y-W, Zhang Y, Jin X-L, Ma Y-Q (2006) Effect of rainfall on stability of anisotropic soil slope. *Rock Soil Mech* 27(Supp.):1097–1102. <https://doi.org/10.16285/j.rsm.2006.s2.098>
- Fitzpatrick EA (1993) *Soil microscopy and micromorphology*. Wiley, Chichester
- Gao G (1996) The distribution and geotechnical properties of loess soils, lateritic soils and clayey soils in China. *Eng Geol* 42:95–104. [https://doi.org/10.1016/0013-7952\(95\)00056-9](https://doi.org/10.1016/0013-7952(95)00056-9)
- Greene-Kelly R, Mackney D (1970) Preferred orientation of clay in soils: the effect of drying and wetting. *Tech Monogr Soil Surv Engl Wales* 2:43–52
- Hao JR, Li DK (1988) An improvement for the determination of permeability coefficient of loess in different directions. *Dam Obs Geotech Tests* 2:37–41
- He B-S, Ding L-Q (2006) Effect of hydraulic seepage anisotropy on the stability of earth dams. *J Chin Inst Water Res Hydropower Res* 4(4):277–281. <https://doi.org/10.13244/j.cnki.jiwhr.2006.04.007>
- He Z-B, Zhao W-Z (2007) Measurement of streambed hydraulic conductivity and anisotropy analysis. *Adv Water Sci* 18(03):351–355. <https://doi.org/10.14042/j.cnki.32.1309.2007.03.007>
- Hong B, Li X-A, Chen G-D, Luo J-W, Li L-C (2016) Experimental study of permeability of remolded Malan loess. *J Eng Geol* 24(02):276–283. <https://doi.org/10.13544/j.cnki.jeg.2016.02.014>
- Hou X, Vanapalli SK, Li T (2018) Water infiltration characteristics in loess associated with irrigation activities and its influence on the slope stability in Heifangtai loess highland, China. *Eng Geol* 234:27–37. <https://doi.org/10.1016/j.enggeo.2017.12.020>
- Hu W, Shao M, Wang Q, Fan J, Horton R (2009) Temporal changes of soil hydraulic properties under different land uses. *Geoderma* 149:355–366. <https://doi.org/10.1016/j.geoderma.2008.12.016>
- Huang D-Z, Xie K-H, Ying H-W (2014) Semi-analytical solution for two-dimensional steady seepage around foundation pit in soil layer with anisotropic permeability. *J Zhejiang Univ (Eng Sci)* 48(10):1802–1808. <https://doi.org/10.3785/j.issn.1008-973X.2014.10.013>
- Jakobson B (1955) Isotropy of clays. *Géotechnique* 5:23–28. <https://doi.org/10.1680/geot.1955.5.1.23>
- Jiang X-W, Wan L, Yeh T-CJ, Wang X-S, Xu L (2010) Steady-state discharge into tunnels in formations with random variability and depth-decaying trend of hydraulic conductivity. *J Hydrol* 387:320–327. <https://doi.org/10.1016/j.jhydrol.2010.04.024>
- Kenney TC, Chan HT (1973) Field investigation of permeability ratio of New Liskeard varved soil. *Can Geotech J* 10:473–488. <https://doi.org/10.1139/t73-039>
- Kie TT (1988) Fundamental properties of loess from Northwestern China. *Eng Geol* 25:103–122. [https://doi.org/10.1016/0013-7952\(88\)90022-1](https://doi.org/10.1016/0013-7952(88)90022-1)
- Lei XY (2001) *Geo-hazards in Loess Plateau and human activity*. Science Press, Beijing
- Leng Y, Peng J, Wang Q, Meng Z, Huang W (2018) A fluidized landslide occurred in the Loess Plateau: a study on loess landslide in South Jingyang tableland. *Eng Geol* 236:129–136. <https://doi.org/10.1016/j.enggeo.2017.05.006>
- Leroueil S, Bouclin G, Tavenas F, Bergeron L, Rochelle PL (1990) Permeability anisotropy of natural clays as a function of strain. *Can Geotech J* 27:568–579. <https://doi.org/10.1139/t90-072>
- Li X-A, Li L-C (2017) Quantification of the pore structures of Malan loess and the effects on loess permeability and environmental significance, Shaanxi Province, China: an experimental study. *Environ Earth Sci* 76:523. <https://doi.org/10.1007/s12665-017-6855-7>
- Li Z, Zheng F-L, Liu W-Z, Jiang D-J (2012) Spatially downscaling GCMs outputs to project changes in extreme precipitation and temperature events on the Loess Plateau of China during the 21st century. *Global Planet Change* 82–83:65–73. <https://doi.org/10.1016/j.gloplacha.2011.11.008>
- Li X-A, Hong B, Li L-C, Wang L (2017) Experimental research on permeability coefficient under influence of loess collapsibility. *China J Highway Transp* 30(6):198–208+222. <https://doi.org/10.19721/j.cnki.1001-7372.2017.06.002>
- Li X-A, Li L-C, Song Y-X, Hong B, Wang L, Sun J-Q (2018) Characterization of the mechanisms underlying loess collapsibility for land-creation project in Shaanxi Province, China—a study from a micro perspective. *Eng Geol* 249:77–88. <https://doi.org/10.1016/j.enggeo.2018.12.024>
- Liang Y, Xing X-L, Li T-L, Xu P, Liu S-L (2012) Study of the anisotropic permeability and mechanism of Q₃ loess. *Rock Soil Mech* 33(5):1313–1318. <https://doi.org/10.16285/j.rsm.2012.05.005>
- Liu T, Ding Z (1998) Chinese loess and the paleomonsoon. *Annu Rev Earth Pl Sc* 26:111–145. <https://doi.org/10.1146/annurev.earth.26.1.111>
- Liu Y-Z, Hu M-Y, Shen Y, Xu K (2012) Experiment on the anisotropy of Hangzhou silt. *J Zhejiang Univ Technol* 40(2):188–192
- Lú J, Ke X-M, Zhang X-X, Li X-J (2017) Variability of saturated permeability coefficient of loess slopes in South Jingyang tableland. *Bull Soil Water Conserv* 37(3):254–257. <https://doi.org/10.13961/j.cnki.stbctb.2017.03.043>
- Lumb P, Holt JK (1968) The undrained shear strength of a soft marine clay from Hong Kong. *Géotechnique* 18:25–36. <https://doi.org/10.1680/geot.1968.18.1.25>

- Mast RF, Potter PE (1963) Sedimentary structures, sand shape fabrics, and permeability. II. *J Geol* 71:548–565. <https://doi.org/10.1086/626932>
- Meade RH (1966) Factors influencing the early stages of the compaction of clays and sands—review. *J Sediment Res* 36(4):1085–1101. <https://doi.org/10.1306/74D71604-2B21-11D7-8648000102C1865D>
- Messing I, Jarvis NJ (1993) Temporal variation in the hydraulic conductivity of a tilled clay soil as measured by tension infiltrometers. *J Soil Sci* 44:11–24. <https://doi.org/10.1111/j.1365-2389.1993.tb00430.x>
- Moench AF (1995) Combining the Neuman and Boulton models for flow to a well in an unconfined aquifer. *Groundwater* 33:378–384. <https://doi.org/10.1111/j.1745-6584.1995.tb00293.x>
- Moon CF (1972) The microstructure of clay sediments. *Earth Sci Rev* 8:303–321. [https://doi.org/10.1016/0012-8252\(72\)90112-2](https://doi.org/10.1016/0012-8252(72)90112-2)
- Northey RD (1969) Engineering properties of loess and other collapsible soils. In: Seventh international conference on soil mechanics and foundation engineering, Mexico City, vol 3, pp 445–452 (**special session 5**)
- Petersen CT, Trautner A, Hansen S (2008) Spatio-temporal variation of anisotropy of saturated hydraulic conductivity in a tilled sandy loam soil. *Soil Tillage Res* 100:108–113. <https://doi.org/10.1016/j.still.2008.05.004>
- Pye K (1984) Loess. *Prog Phys Geogr* 8:176–217. <https://doi.org/10.1177/030913338400800202>
- Qi L, Liao H, Li L (2012) Influence analysis of seepage boundary conditions of anisotropy in rock-soil body Gate Dam Foundation. *Water Res Power* 30(8):56–58+15
- Qian J-G, Huang M-S (2011) Micro–macro mechanistic analysis of plastic anisotropy in soil. *Rock Soil Mech* 32(Supp. 2):88–93. <https://doi.org/10.16285/j.rsm.2011.s2.013>
- Rogers CDF, Dijkstra TA, Smalley IJ (1994) Hydroconsolidation and subsidence of loess: studies from China, Russia, North America and Europe: In memory of Jan Sajgalik. *Eng Geol* 37:83–113. [https://doi.org/10.1016/0013-7952\(94\)90045-0](https://doi.org/10.1016/0013-7952(94)90045-0)
- Shakir RR (2009) Quantity of flow through a typical dam of anisotropic permeability. In: Yuan Y, Cui JZ, Mang HA (eds) Computational structural engineering. Springer, Dordrecht, pp 1301–1308. https://doi.org/10.1007/978-90-481-2822-8_147
- Sheeler JB (1968) Summarization and comparison of engineering properties of loess in the United States. *Highway Research Record*, pp 1–9
- Tavenas F, Jean P, Leblond P, Leroueil S (1983) The permeability of natural soft clays. Part II: permeability characteristics. *Can Geotech J* 20:645–660. <https://doi.org/10.1139/t83-073>
- Teufel LW, Rhett DW, Farrell HE, Lorenz JC (1993) Control of fractured reservoir permeability by spatial and temporal variations in stress magnitude and orientation. Paper presented at the SPE Annual Technical Conference and Exhibition, Houston, TX. <https://doi.org/10.2118/26437-MS>
- Van Olphen H (1963) An introduction to clay colloid chemistry. Interscience, New York
- Wang M, Bai X-H, Yang J (2010) Method of specimen preparation for collapsible loess microstructure research. *J Taiyuan Univ Technol* 41(3):283–286. <https://doi.org/10.16355/j.cnki.issn1007-9432t.yt.2010.03.018>
- Wang C, Ding W, Liu S, Wang J, Tang Z (2014) Analysis of dynamic changes of anisotropic permeability coefficient with volumetric strain in seepage coupling. *Chin J Rock Mech Eng* 33(S1):3015–3021. <https://doi.org/10.13722/j.cnki.jrme.2014.s1.060>
- Wang L, Wang S, Xiang L (2015) Preferential flow analysis of a clayey soil landslide under rainfall in three gorges reservoir area. *Chin J Undergr Space Eng* 11(4):1047–1052
- Wang T-X, Yang T, Lu J (2016) Influence of dry density and freezing-thawing cycles on anisotropic permeability of loess. *Rock Soil Mech* 37(Supp. 1):72–78. <https://doi.org/10.16285/j.rsm.2016.S1.009>
- Wang W, Wang Y, Sun Q, Zhang M, Qiang Y, Liu M (2018) Spatial variation of saturated hydraulic conductivity of a loess slope in the South Jingyang Plateau, China. *Eng Geol* 236:70–78. <https://doi.org/10.1016/j.enggeo.2017.08.002>
- Widdowson MA, Molz FJ, Melville JG (1990) An analysis technique for multilevel and partially penetrating slug test data. *Groundwater* 28:937–945. <https://doi.org/10.1111/j.1745-6584.1990.tb01730.x>
- Witt KJ, Brauns J (1983) Permeability-anisotropy due to particle shape. *J Geotech. Eng* 109:1181–1187. [https://doi.org/10.1061/\(ASCE\)0733-9410\(1983\)109:9\(1181\)](https://doi.org/10.1061/(ASCE)0733-9410(1983)109:9(1181))
- Yang T (2016) Study on anisotropic permeability of loess considering density and freezing-thawing effect. Dissertation, Xi'an University of Architecture and Technology
- Yu, X (2016) The anisotropy and the scale effect of hydraulic conductivity for the loess in Baoji city, Shaanxi Province. Dissertation, Chang'an University
- Zeng C, Wang Q, Zhang F, Zhang J (2013) Temporal changes in soil hydraulic conductivity with different soil types and irrigation methods. *Geoderma* 193–194:290–299. <https://doi.org/10.1016/j.geoderma.2012.10.013>
- Zhang L-W (2011) Study on the effect of strength anisotropy on the stability of soil slopes. *China Min Mag* 20(12):108–110
- Zhang X-X (2016) Characteristics of loess saturated hydraulic conductivity in landslide of the south Jingyang Plateau. Dissertation, Chang'an University
- Zhang Z-H, Yao Z-J, Wang K-S (1973) Main engineering geological problems of Chinese loess. *Acta Geol Sin* 2:255–269
- Zhang R, Yue L, Gong H, Zhang Y, Li J (2012) Anisotropy of magnetic susceptibility of Eolian sediments in the Chinese Loess Plateau. *Quat Sci* 32(04):719–726. <https://doi.org/10.3969/j.issn.1001-7410.2012.04.17>
- Zhang F, Pei X, Chen W, Liu G, Liang S (2014) Spatial variation in geotechnical properties and topographic attributes on the different types of shallow landslides in a loess catchment, China. *Eur J Environ Civ Eng* 18:470–488. <https://doi.org/10.1080/19648189.2014.881754>
- Zhang DM, Ma LX, Zhang J, Hicher PY, Juang CH (2015) Ground and tunnel responses induced by partial leakage in saturated clay with anisotropic permeability. *Eng Geol* 189:104–115. <https://doi.org/10.1016/j.enggeo.2015.02.005>
- Zhang S, Tang H, Liu X, Tan Q, Xiahou Y (2018) Seepage and instability characteristics of slope based on spatial variation structure of saturated hydraulic conductivity. *Earth Sci* 43(2):622–634. <https://doi.org/10.3799/dqkx.2017.617>
- Zhuang J, Peng J, Xu Y, Xu Q, Zhu X, Li W (2016) Assessment and mapping of slope stability based on slope units: a case study in Yan'an, China. *J Earth Syst Sci* 125:1439–1450. <https://doi.org/10.1007/s12040-016-0741-7>
- Zhuang J, Peng J, Wang G, Iqbal J, Wang Y, Li W, Xu Q, Zhu X (2017) Prediction of rainfall-induced shallow landslides in the Loess Plateau, Yan'an, China, using the TRIGRS model. *Earth Surf Proc Land* 42:915–927. <https://doi.org/10.1002/esp.4050>
- Zhuang J, Peng J, Wang G, Javed I, Wang Y, Li W (2018) Distribution and characteristics of landslide in Loess Plateau: a case study in Shaanxi province. *Eng Geol* 236:89–96. <https://doi.org/10.1016/j.enggeo.2017.03.001>

Publisher's Note Springer Nature remains neutral with regard to jurisdictional claims in published maps and institutional affiliations.